Inverse Problems and Imaging
Vol. 23, 2026, pp. 51-69 (October 31, 2025)
doi:10.3934/ipi.2025054

FACTORIZATION METHOD FOR NEAR-FIELD INVERSE SCATTERING PROBLEMS IN ELASTODYNAMICS

Chun Liu[✉,1], Guanghui Hu[✉,1], Tao Yin[✉,2] and Bo Zhang[✉,2,3]

[1]School of Mathematical Sciences and LPMC, Nankai University, Tianjing 300071, China

[2]State Key Laboratory of Mathematical Sciences, Academy of Mathematics and Systems Science, Chinese Academy of Sciences, Beijing 100190, China

[3]School of Mathematical Sciences, University of Chinese Academy of Sciences, Beijing 100049, China

(Communicated by Xiang Xu)

Abstract. Consider a time-harmonic elastic wave scattering problem with a bounded rigid obstacle embedded in a homogeneous and isotropic elastic medium. This work is concerned with the inverse problem of recovering the location and shape of the obstacle from near-field data generated by infinitely many incident point source waves at a fixed energy. An outgoing-to-incoming operator is defined for facilitating the factorization of the near-field operator. Necessary properties of the factorization of the composition of the outgoing-to-incoming operator and the near-field operator are shown to apply the range identity to construct an indicator function for the reconstruction. Numerical examples in 2D are presented to show the validity and accuracy of the inversion algorithm.

1. **Introduction.** The obstacle scattering problem is one of the fundamental scattering problems in physics. The direct obstacle scattering problem involves determining the scattered field from the known obstacle and given incident field, while the inverse obstacle scattering problem aims to reconstruct the shape and location of the obstacle from the measurement of the scattered field. It has been widely studied due to its diverse applications in many scientific areas [21, 22], such as radar and sonar, medical imaging and geophysical exploration [2, 8]. Unlike acoustic and electromagnetic waves, elastic wave is governed by the Navier equation, which is more complex due to the coupling of longitudinal and transverse waves that propagate at different speeds. Therefore, it presents challenges for inverse elastic obstacle scattering problem on both mathematical analysis and computation.

Over the past few decades, significant progress has been made in both theoretical analysis and numerical methods for the inverse elastic obstacle scattering problem. The uniqueness results using infinitely many incident plane waves have been established in [9, 10] with full-phase far-field data and in [5] using phaseless far-field data with a reference ball. Additionally, uniqueness results using infinitely

2020 *Mathematics Subject Classification.* Primary: 35R30, 74J25.

Key words and phrases. Factorization method, inverse scattering, near-field data, Navier equation, point sources.

many incident point sources were obtained in [1] with near-field data. Similar to the acoustic case, this uniqueness result with near-field data could also be easily proved by using Rellich's lemma and the mixed reciprocity relation for elastic waves. The numerical methods can be broadly classified into two types: the quantitative method and the qualitative method. Quantitative methods, such as optimization-based iterative approaches, include the domain derivatives [17], the continuation method [26]. Qualitative methods, imaging based direct method, refers to the sampling method and its variants, such as the linear sampling method [3], the direct sampling method [13], and the factorization method [7, 19, 24]. While iterative methods require prior information about the geometry and physical properties of the obstacle and involve solving adjoint direct scattering problems at each iteration, sampling methods overcome these difficulties but may yield less accurate reconstructions compared to iterative methods.

The basic idea of the sampling methods is to design an indicator function which attains large values inside the underlying scatterer and relative small values outside. In all of the sampling methods, the measurements may be divided into two types: far-field data and near-field data. However, the theoretical analysis for far-field data is more developed than that for near-field data. For the near-field case, [11] established the factorization method for the near-field operator by introducing the outgoing-to-incoming(OtI) operator. In their work, the OtI operator for the Helmholtz equation was constructed on a spherical surface and the factorization method worked for recovering both impenetrable and penetrable scatterers. This approach was later extended by [25] to the inverse fluid-solid interaction problem with non-spherical measurement surface. Additionally, [12] established a direct sampling method using near-field measurements for inverse acoustic obstacle scattering, and [20] proposed a modified sampling method applicable to inverse acoustic cavity scattering problems.

The factorization method was first elaborated for the shape reconstruction of an acoustically soft or hard scatterer in the original paper [14] and has been extended and developed since then [15]. It provides an explicit characterization of the scattering obstacle which uses only the spectral system of the well-known far-field operator. As far as inverse elastic scattering problems via the factorization method is concerned, the number of available results is much smaller when compared with its counterpart in acoustics. In this paper, we consider an inverse elastic scattering problem of determining the shape and location of an obstacle using the factorization method with near-field measurement data. The obstacle is assumed to be an elastically rigid body embedded in an open space filled with a homogeneous and isotropic elastic medium. Both the incident point sources and the receivers for measuring the scattered field are located on a spherical closed surface. Motivated by the works of [11] and [25], we propose a factorization method for this inverse problem. We give an explicit expansion of the scattered field and fundamental solution to the Navier equation. Then we define and illustrate properties of the OtI operator and its adjoint operator. Finally, the near-field operator defined on a spherical measurement surface is modified by the OtI operator such that possesses a symmetric factorization similar to the factorization of the far-field operator case can be achieved.

The paper is organized as follows: In Section 2, we formulate the problem in three dimensions. Section 3 introduces the definition of the outgoing-to-incoming

operator and the factorization of the modified near-field operator. Finally, Section 4 presents numerical experiments conducted in two dimensions to validate the proposed method.

2. **Problem formulation.** This paper is concerned with the time-harmonic scattering of elastic waves by a bounded rigid obstacle at a fixed frequency. Our analysis will be mainly performed in 3D case, which can be carried over to 2D. Denote by $D \subset \mathbb{R}^3$ a bounded obstacle with C^2-smooth boundary ∂D. The exterior $D^c := \mathbb{R}^3 \setminus \overline{D}$, assumed to be connected, is characterized by a mass density $\rho > 0$ and Lamé constants λ and μ, satisfying $\mu > 0$ and $2\mu + 3\lambda > 0$. Without loss of generality, we set $\rho \equiv 1$ in $\mathbb{R}^3$. Let $B_R := \{\boldsymbol{x} = (x_1, x_2, x_3)^\top \in \mathbb{R}^3 : |\boldsymbol{x}| < R\}$ be a ball of radius $R > 0$ such that $\overline{D} \subset B_R$, and let $S_R := \{\boldsymbol{x} \in \mathbb{R}^3 : |\boldsymbol{x}| = R\}$ denote the boundary of B_R. Here $(\cdot)^\top$ represents the transpose of a vector or a matrix. We write the unit sphere in $\mathbb{R}^3$ as $\mathbb{S}^2 := \{\boldsymbol{x} \in \mathbb{R}^3 : |\boldsymbol{x}| = 1\}$.

The propagation of time-harmonic elastic waves in D^c is governed by the time-harmonic Navier equation

$$\Delta^* \boldsymbol{u} + \omega^2 \boldsymbol{u} = \boldsymbol{0}, \quad \boldsymbol{x} \in D^c, \qquad \Delta^* = \mu\Delta + (\lambda + \mu)\nabla(\nabla\cdot), \tag{1}$$

where $\boldsymbol{u}$ represents the scattered field and the angular frequency $\omega > 0$ is constant. The solution $\boldsymbol{u}$ of (1) can be decomposed into a sum of compressional and shear waves,

$$\boldsymbol{u} = \boldsymbol{u}_p + \boldsymbol{u}_s, \ \boldsymbol{u}_p = -k_p^{-2}\nabla(\nabla \cdot \boldsymbol{u}), \quad \boldsymbol{u}_s = -k_s^{-2}\nabla \times (\nabla \times \boldsymbol{u}),$$

where $k_p := \omega/\sqrt{2\mu + \lambda}$, $k_s := \omega/\sqrt{\mu}$ are the compressional and shear wave numbers, respectively. The components $\boldsymbol{u}_p$ and $\boldsymbol{u}_s$ satisfy the vector Helmholtz equations

$$\Delta \boldsymbol{u}_p + k_p^2 \boldsymbol{u}_p = \boldsymbol{0}, \qquad \Delta \boldsymbol{u}_s + k_s^2 \boldsymbol{u}_s = \boldsymbol{0}, \qquad \boldsymbol{x} \in D^c.$$

Since the obstacle is elastically rigid, we impose the inhomogeneous Dirichlet boundary condition

$$\boldsymbol{u} = -\boldsymbol{u}^{in}, \qquad \boldsymbol{x} \in \partial D, \tag{2}$$

where $\boldsymbol{u}^{in}$ is the incident field. The surface stress (or traction) operator T on the boundary ∂D is defined as

$$T\boldsymbol{u} = 2\mu \boldsymbol{n} \cdot \nabla \boldsymbol{u} + \lambda \boldsymbol{n} \nabla \cdot \boldsymbol{u} + \mu \boldsymbol{n} \times \nabla \times \boldsymbol{u},$$

where $\boldsymbol{n}$ is the unit normal vector on ∂D directed into the exterior of D.

In this work, we consider the point source incident wave $\boldsymbol{u}^{in}(\boldsymbol{x}, \boldsymbol{y}; \boldsymbol{a})$ with the polarization direction $\boldsymbol{a} \in \mathbb{S}^2$:

$$\boldsymbol{u}^{in}(\boldsymbol{x}, \boldsymbol{y}; \boldsymbol{a}) = \Pi(\boldsymbol{x}, \boldsymbol{y})\boldsymbol{a}, \qquad \boldsymbol{x} \neq \boldsymbol{y}, \ \boldsymbol{y} \in D^c,$$

where $\Pi(\boldsymbol{x}, \boldsymbol{y})$ is the free-space Green's tensor to the Navier equation, given by

$$\Pi(\boldsymbol{x}, \boldsymbol{y}) = \frac{1}{\mu}\Phi_{k_s}(\boldsymbol{x}, \boldsymbol{y})\mathbf{I} + \frac{1}{\omega^2}\nabla_{\boldsymbol{x}}\nabla_{\boldsymbol{x}}^\top[\Phi_{k_s}(\boldsymbol{x}, \boldsymbol{y}) - \Phi_{k_p}(\boldsymbol{x}, \boldsymbol{y})], \qquad \boldsymbol{x} \neq \boldsymbol{y}.$$

Here, $\mathbf{I}$ stands for the 3×3 identity matrix, $\Phi_k(\boldsymbol{x}, \boldsymbol{y}) = \exp(ik|\boldsymbol{x} - \boldsymbol{y}|)/(4\pi|\boldsymbol{x} - \boldsymbol{y}|)$ is the free-space fundamental solution to the Helmholtz equation $(\Delta + k^2)u = 0$ in $\mathbb{R}^3$. The scattered field corresponding to $\boldsymbol{u}^{in}(\boldsymbol{x}, \boldsymbol{y}; \boldsymbol{a})$ is denoted as $\boldsymbol{u} = \boldsymbol{u}(\boldsymbol{x}, \boldsymbol{y}; \boldsymbol{a})$.

To ensure the wellposedness of the direct problem, the scattered field $\boldsymbol{u}$ is required to satisfy the Kupradze radiation condition

$$\lim_{r=|\boldsymbol{x}|\to\infty} r\left[\frac{\partial \boldsymbol{u}_\alpha(\boldsymbol{x})}{\partial r} - ik_\alpha \mathbf{u}_\alpha(\boldsymbol{x})\right] = 0, \qquad \alpha = p, s, \tag{3}$$

uniformly in all directions $\hat{\boldsymbol{x}} = \boldsymbol{x}/|\boldsymbol{x}| \in \mathbb{S}^2$. This condition (3) is known as the Sommerfeld condition for the compressional and shear parts of $\boldsymbol{u}$ [16].

Given the incident field $\boldsymbol{u}^{in}$, the *direct scattering problem* (DP) for (1) – (3) is to find the scattered field $\boldsymbol{u}$ for a known obstacle D. By using variational approach in combination with properties of transparent operator for the Navier equation (1), [4, 18] shows that the problem (DP) admits at most one solution $\boldsymbol{u} \in [H^1_{loc}(D^c)]^3$. The existence of a solution to the problem (DP) was proved in Theorem 1 in [9] via the integral equation method. The inverse scattering problem is to reconstruct the shape and location of the obstacle D from the near-field data $\{\boldsymbol{u}(\boldsymbol{x}, \boldsymbol{y}; \boldsymbol{a_i}) : \boldsymbol{x}, \boldsymbol{y} \in S_R, \boldsymbol{a_i} \in \mathbb{S}^2, i = 1, 2, 3\}$, where $\boldsymbol{a_i}$ $(i = 1, 2, 3)$ are three linearly independent polarizations. Theorem 3 and Theorem 4 in [9] prove that the far-field data for incident plane waves $\boldsymbol{u}^{in}(\boldsymbol{x}) = \boldsymbol{d}\exp(ik_p\boldsymbol{d}\cdot\boldsymbol{x}) + \boldsymbol{q}\exp(ik_s\boldsymbol{d}\cdot\boldsymbol{x})$ for all $\boldsymbol{d}, \boldsymbol{q} \in \mathbb{S}^2$, $\boldsymbol{d}\cdot\boldsymbol{q} = 0$ at a fixed frequency ω can uniquely determine the scatterer D. By using Rellich's lemma and the mixed reciprocity relation (see [23]), we can obtain that the near-field data for incident point source can uniquely reconstruct the obstacle D.

3. Factorization of near-field operator.

For $\boldsymbol{g} \in [L^2(S_R)]^3$, we define the incident field $\boldsymbol{v}^{in}_{\boldsymbol{g}}$ as

$$\boldsymbol{v}^{in}_{\boldsymbol{g}}(\boldsymbol{x}) = \int_{S_R} \Pi(\boldsymbol{x}, \boldsymbol{y})\boldsymbol{g}(\boldsymbol{y})\mathrm{d}s(\boldsymbol{y}), \qquad \boldsymbol{x} \in \mathbb{R}^3. \tag{4}$$

The scattered field corresponding to $\boldsymbol{v}^{in}_{\boldsymbol{g}}$ takes the form

$$\boldsymbol{v}_{\boldsymbol{g}}(\boldsymbol{x}) = \int_{S_R} \boldsymbol{u}(\boldsymbol{x}, \boldsymbol{y}; \boldsymbol{g}(\boldsymbol{y}))\mathrm{d}s(\boldsymbol{y}), \qquad \boldsymbol{x} \in D^c, \tag{5}$$

where $\boldsymbol{u}(\boldsymbol{x}, \boldsymbol{y}; \boldsymbol{g}(\boldsymbol{y}))$ represents the scattered field generated by incident field $\Pi(\boldsymbol{x}, \boldsymbol{y})$ $\boldsymbol{g}(\boldsymbol{y})$. Then we can define the near-field operator $N : [L^2(S_R)]^3 \to [L^2(S_R)]^3$ by

$$(N\boldsymbol{g})(\boldsymbol{x}) = \int_{S_R} \boldsymbol{u}(\boldsymbol{x}, \boldsymbol{y}; \boldsymbol{g}(\boldsymbol{y}))\mathrm{d}s(\boldsymbol{y}), \qquad \boldsymbol{x} \in S_R. \tag{6}$$

Clearly, $N\boldsymbol{g}$ is the restriction to S_R of the scattered field $\boldsymbol{v}_{\boldsymbol{g}}$ generated by the incident wave $\boldsymbol{v}^{in}_{\boldsymbol{g}}$.

In this section, we will establish a factorization of the near-field operator N for incident point sources. Motivated by [11] in acoustics, we first introduce the elastic OtI operator $\mathcal{T}$ and then get a symmetric factorization of the product operator $\mathcal{T}N$.

3.1. Solution operator.

Definition 3.1. Given $\boldsymbol{h} \in [H^{\frac{1}{2}}(\partial D)]^3$, denoted by $\boldsymbol{v} \in [H^1_{loc}(D^c)]^3$ the unique solution to the boundary value problem

$$\begin{aligned} \Delta^*\boldsymbol{v} + \omega^2\boldsymbol{v} &= \boldsymbol{0}, \quad \boldsymbol{x} \in D^c, \\ \boldsymbol{v} &= \boldsymbol{h}, \qquad \boldsymbol{x} \in \partial D, \end{aligned}$$

and that $\boldsymbol{v}$ satisfies the Kupradze radiation condition (3). The solution operator is defined as $G : [H^{\frac{1}{2}}(\partial D)]^3 \to [L^2(S_R)]^3$

$$G\boldsymbol{h} = \boldsymbol{v}|_{S_R}. \tag{7}$$

Clearly, G maps the boundary value of a radiating solution on ∂D onto the near-field pattern on S_R.

Theorem 3.2. *The solution operator $G : [H^{\frac{1}{2}}(\partial D)]^3 \to [L^2(S_R)]^3$ is compact, injective with a dense range in $[L^2(S_R)]^3$.*

Proof. The injectivity of G follows from the uniqueness of the exterior Dirichlet problem [9] and the analytic continuation argument. The compactness of G follows from the fact that the scattering problem (1) – (3) has a solution $\boldsymbol{u} \in [H^1_{loc}(D^c)]^3$, and $[H^{\frac{1}{2}}(S_R)]^3$ can be compactly embedded into $[L^2(S_R)]^3$.

Denote $\boldsymbol{u}$ the unique solution to the scattering problem (1) – (3) with the boundary value $\boldsymbol{u} = \boldsymbol{f} \in [H^{\frac{1}{2}}(\partial D)]^3$. Then $\boldsymbol{u}$ can be expressed as

$$\boldsymbol{u}(\boldsymbol{x}) = \int_{\partial D} \{T\Pi(\boldsymbol{x}, \boldsymbol{y}) \cdot \boldsymbol{u}(\boldsymbol{y}) - \Pi(\boldsymbol{x}, \boldsymbol{y}) \cdot T\boldsymbol{u}(\boldsymbol{y})\} \mathrm{d}s(\boldsymbol{y}), \qquad \boldsymbol{x} \in D^c. \tag{8}$$

Then one has for $\boldsymbol{g} \in [L^2(S_R)]^3$ that

$$\begin{aligned} (G\boldsymbol{f}, \boldsymbol{g})_{[L^2(S_R)]^3} &= \int_{S_R} \boldsymbol{u}(\boldsymbol{x}) \cdot \overline{\boldsymbol{g}}(\boldsymbol{x}) \mathrm{d}s(\boldsymbol{x}) \\ &= \int_{\partial D} \{\boldsymbol{u}(\boldsymbol{y}) \cdot T\boldsymbol{v}^{in}_{\overline{\boldsymbol{g}}}(\boldsymbol{y}) - T\boldsymbol{u}(\boldsymbol{y}) \cdot \boldsymbol{v}^{in}_{\overline{\boldsymbol{g}}}(\boldsymbol{y})\} \mathrm{d}s(\boldsymbol{y}). \end{aligned} \tag{9}$$

As both $\boldsymbol{u}$ and $\boldsymbol{v}_{\overline{\boldsymbol{g}}}$ are radiating solutions, we find

$$\int_{\partial D} \{\boldsymbol{u}(\boldsymbol{y}) \cdot T\boldsymbol{v}_{\overline{\boldsymbol{g}}}(\boldsymbol{y}) - T\boldsymbol{u}(\boldsymbol{y}) \cdot \boldsymbol{v}_{\overline{\boldsymbol{g}}}(\boldsymbol{y})\} \mathrm{d}s(\boldsymbol{y}) = 0. \tag{10}$$

Using the boundary condition $\boldsymbol{v}^{in}_{\overline{\boldsymbol{g}}} + \boldsymbol{v}_{\overline{\boldsymbol{g}}} = \boldsymbol{0}$, we derive form (9) and (10) that

$$\begin{aligned} (G\boldsymbol{f}, \boldsymbol{g})_{[L^2(S_R)]^3} &= \int_{\partial D} \boldsymbol{u}(\boldsymbol{y}) \cdot T\left(\boldsymbol{v}^{in}_{\overline{\boldsymbol{g}}}(\boldsymbol{y}) + \boldsymbol{v}_{\overline{\boldsymbol{g}}}(\boldsymbol{y})\right) \mathrm{d}s(\boldsymbol{y}) \\ &= \int_{\partial D} \boldsymbol{f}(\boldsymbol{y}) \cdot T\left(\boldsymbol{v}^{in}_{\overline{\boldsymbol{g}}}(\boldsymbol{y}) + \boldsymbol{v}_{\overline{\boldsymbol{g}}}(\boldsymbol{y})\right) \mathrm{d}s(\boldsymbol{y}). \end{aligned}$$

As a result, the adjoint operator G^* can be characterized as $G^*\boldsymbol{g} = \overline{T\left(\boldsymbol{v}^{in}_{\overline{\boldsymbol{g}}} + \boldsymbol{v}_{\overline{\boldsymbol{g}}}\right)}$. If $G^*\boldsymbol{g} = \boldsymbol{0}$, then $T\left(\boldsymbol{v}^{in}_{\overline{\boldsymbol{g}}} + \boldsymbol{v}_{\overline{\boldsymbol{g}}}\right) = \boldsymbol{0}$, which implies that $T\boldsymbol{v}_{\overline{\boldsymbol{g}}} = -T\boldsymbol{v}^{in}_{\overline{\boldsymbol{g}}}$ on ∂D. By virtue of (8) and the boundary condition $\boldsymbol{v}^{in}_{\overline{\boldsymbol{g}}} = -\boldsymbol{v}_{\overline{\boldsymbol{g}}} = \boldsymbol{0}$ on ∂D, one finds that

$$\boldsymbol{v}_{\overline{\boldsymbol{g}}}(\boldsymbol{x}) = -\int_{\partial D} \{T\Pi(\boldsymbol{x}, \boldsymbol{y}) \cdot \boldsymbol{v}^{in}_{\overline{\boldsymbol{g}}}(\boldsymbol{y}) - \Pi(\boldsymbol{x}, \boldsymbol{y}) \cdot T\boldsymbol{v}^{in}_{\overline{\boldsymbol{g}}}(\boldsymbol{y})\} \mathrm{d}s(\boldsymbol{y}), \qquad \boldsymbol{x} \in D^c.$$

Since both $\boldsymbol{v}^{in}_{\overline{\boldsymbol{g}}}$ and $\boldsymbol{y} \to \Pi(\boldsymbol{x}, \boldsymbol{y})$ for $\boldsymbol{x} \in D^c$ satisfy the Navier equation in D, the Betti's formula applied over D shows that

$$\begin{aligned} &-\boldsymbol{v}_{\overline{\boldsymbol{g}}}(\boldsymbol{x}) \\ =&\int_{\partial D} \{T\Pi(\boldsymbol{x}, \boldsymbol{y}) \cdot \boldsymbol{v}^{in}_{\overline{\boldsymbol{g}}}(\boldsymbol{y}) - \Pi(\boldsymbol{x}, \boldsymbol{y}) \cdot T\boldsymbol{v}^{in}_{\overline{\boldsymbol{g}}}(\boldsymbol{y})\} \mathrm{d}s(\boldsymbol{y}) \\ =&\int_D \{\Delta^*\Pi(\boldsymbol{x}, \boldsymbol{y}) \cdot \boldsymbol{v}^{in}_{\overline{\boldsymbol{g}}}(\boldsymbol{y}) - \Pi(\boldsymbol{x}, \boldsymbol{y}) \cdot \Delta^*\boldsymbol{v}^{in}_{\overline{\boldsymbol{g}}}(\boldsymbol{y})\} \mathrm{d}\boldsymbol{y} \\ =&\int_D \{(\Delta^*\Pi(\boldsymbol{x}, \boldsymbol{y}) + \omega^2\Pi(\boldsymbol{x}, \boldsymbol{y})) \cdot \boldsymbol{v}^{in}_{\overline{\boldsymbol{g}}}(\boldsymbol{y}) - \Pi(\boldsymbol{x}, \boldsymbol{y}) \cdot (\Delta^*\boldsymbol{v}^{in}_{\overline{\boldsymbol{g}}}(\boldsymbol{y}) + \omega^2\boldsymbol{v}^{in}_{\overline{\boldsymbol{g}}}(\boldsymbol{y}))\} \mathrm{d}\boldsymbol{y} \\ =&\boldsymbol{0}, \end{aligned}$$

for all $\boldsymbol{x} \in D^c$. Thus $\boldsymbol{v}_{\overline{\boldsymbol{g}}}(\boldsymbol{x}) = T\boldsymbol{v}_{\overline{\boldsymbol{g}}}(\boldsymbol{x}) = \boldsymbol{0}$ on ∂D, which means that $\boldsymbol{v}^{in}_{\overline{\boldsymbol{g}}}(\boldsymbol{x}) = T\boldsymbol{v}^{in}_{\overline{\boldsymbol{g}}}(\boldsymbol{x}) = \boldsymbol{0}$ on ∂D. Using the Holmgren's uniqueness theorem, one finds that $\boldsymbol{v}^{in}_{\overline{\boldsymbol{g}}} = \boldsymbol{0}$ in $\mathbb{R}^3$. The jump relation shows that $\boldsymbol{g} = T(\boldsymbol{v}^{in}_{\overline{\boldsymbol{g}}})^- - T(\boldsymbol{v}^{in}_{\overline{\boldsymbol{g}}})^+$, where the superscripts $'-'$ and $'+'$ denote respectively the limits from inside and outside of B_R. Thus $\boldsymbol{g} = \boldsymbol{0}$, which means that G^* is injective. Hence G has dense range by Theorem 4.6 in [6]. □

Define the incidence operator $H : [L^2(S_R)]^3 \to [H^{\frac{1}{2}}(\partial D)]^3$ by

$$(H\boldsymbol{g})(\boldsymbol{x}) = \int_{S_R} \Pi(\boldsymbol{x}, \boldsymbol{y})\boldsymbol{g}(\boldsymbol{y})\mathrm{d}s(\boldsymbol{y}), \qquad \boldsymbol{x} \in \partial D.$$

Since $\Pi(\boldsymbol{x}, \boldsymbol{y}) = \Pi(\boldsymbol{x}, \boldsymbol{y})^\top$, the L^2-adjoint $H^* : [H^{-\frac{1}{2}}(\partial D)]^3 \to [L^2(S_R)]^3$ of H is given by

$$(H^*\boldsymbol{\varphi})(\boldsymbol{x}) = \int_{\partial D} \overline{\Pi(\boldsymbol{x}, \boldsymbol{y})}\boldsymbol{\varphi}(\boldsymbol{y})\mathrm{d}s(\boldsymbol{y}), \qquad \boldsymbol{x} \in S_R.$$

Here, for a matrix $A = (a_{ij})$, we define $\overline{A} := (\overline{a_{ij}})$. From the definition of N, G and H, the following relation holds

$$N = -GH. \tag{11}$$

3.2. **Outgoing-to-incoming (OtI) operator.** In this subsection we give the definition of OtI operator on a spherical surface. Denote (r, θ, φ) the spherical coordinates of $\boldsymbol{x} \in \mathbb{R}^3$, where $\theta \in [0, 2\pi]$ and $\varphi \in [0, \pi]$ are the Euler angles. Let

$$\begin{aligned}
\widehat{\boldsymbol{r}} &= (\sin\theta\cos\varphi, \sin\theta\sin\varphi, \cos\theta)^\top,\\
\widehat{\boldsymbol{\theta}} &= (\cos\theta\cos\varphi, \cos\theta\sin\varphi, -\sin\theta)^\top,\\
\widehat{\boldsymbol{\varphi}} &= (-\sin\varphi, \cos\varphi, 0)^\top
\end{aligned}$$

be the unit vectors in the spherical coordinates. $\{\widehat{\boldsymbol{r}}, \widehat{\boldsymbol{\theta}}, \widehat{\boldsymbol{\varphi}}\}$ forms a local orthonormal basis, and $\widehat{\boldsymbol{r}}$ is the unit outward normal vector on S_R.

Let $\{Y_n^m(\theta, \varphi) : n = 0, 1, 2\ldots, m = -n.\ldots n\}$ be the orthonormal sequence of spherical harmonic functions of order n on the unit sphere. Define the vector spherical harmonics:

$$\begin{aligned}
\boldsymbol{U}_n^m(\widehat{\boldsymbol{x}}) &:= \frac{1}{\sqrt{\delta_n}}\nabla_{\mathbb{S}^2} Y_n^m(\widehat{\boldsymbol{x}}),\\
\boldsymbol{V}_n^m(\widehat{\boldsymbol{x}}) &:= \widehat{\boldsymbol{x}} \times \boldsymbol{U}_n^m(\widehat{\boldsymbol{x}}),\\
\boldsymbol{W}_n^m(\widehat{\boldsymbol{x}}) &:= Y_n^m(\widehat{\boldsymbol{x}})\ \widehat{\boldsymbol{x}},
\end{aligned}$$

where $\widehat{\boldsymbol{x}} := \boldsymbol{x}/|\boldsymbol{x}| \in \mathbb{S}^2$ and $\delta_n := n(n+1), n = 0, 1, 2\ldots, m = -n\ldots n$. Denote by $\nabla_{\mathbb{S}^2}$ the surface gradient on $\mathbb{S}^2$. Set $M_n^m(\widehat{\boldsymbol{x}}) := (\boldsymbol{V}_n^m(\widehat{\boldsymbol{x}}), \boldsymbol{U}_n^m(\widehat{\boldsymbol{x}}), \boldsymbol{W}_n^m(\widehat{\boldsymbol{x}})) \in \mathbb{C}^{3\times 3}$. We can easily show that $\{M_n^m(\theta, \varphi) : n = 0, 1, 2\ldots, m = -n.\ldots n\}$ form a complete orthonormal system in $[L^2(\mathbb{S}^2)]^3$.

The radiating solution $\boldsymbol{u}$ to the Navier equation (1) in $|\boldsymbol{x}| \geq R$ can be expressed as (see [4, Section 2.4])

$$\boldsymbol{u}(\boldsymbol{x}) = \sum_{n=0}^{\infty}\sum_{m=-n}^{n} M_n^m(\widehat{\boldsymbol{x}})A_n(|\boldsymbol{x}|)\boldsymbol{\alpha}_n^m, \tag{12}$$

where $\boldsymbol{\alpha}_n^m \in \mathbb{C}^3$ and $A_n(|\boldsymbol{x}|)$ is defined as

$$\begin{aligned}
&A_n(|\boldsymbol{x}|)\\
&:= \begin{pmatrix}
h_n^{(1)}(k_s|\boldsymbol{x}|) & 0 & 0\\
0 & -\left(h_n^{(1)}(k_s|\boldsymbol{x}|) + k_s|\boldsymbol{x}|h_n^{(1)'}(k_s|\boldsymbol{x}|)\right)/|\boldsymbol{x}| & \sqrt{\delta_n}h_n^{(1)}(k_p|\boldsymbol{x}|)/|\boldsymbol{x}|\\
0 & -\sqrt{\delta_n}h_n^{(1)}(k_s|\boldsymbol{x}|)/|\boldsymbol{x}| & k_p h_n^{(1)'}(k_p|\boldsymbol{x}|)
\end{pmatrix}.
\end{aligned} \tag{13}$$

Here, $h_n^{(1)}$ and $h_n^{(1)'}$ are the spherical Hankel functions of order n and its first derivative, respectively.

Definition 3.3. Let $\boldsymbol{u}$ be an outgoing solution to the problem (1) – (3). Suppose that $\boldsymbol{u}$ admits the expansion (12) for all $|\boldsymbol{x}| \geq R$. Then the OtI mapping $\mathcal{T}$: Range(G) $\to [\mathrm{L}^2(\mathrm{S_R})]^3$ is defined as

$$\mathcal{T}(\boldsymbol{u}|_{S_R}) = \tilde{\boldsymbol{u}}|_{S_R} \tag{14}$$

with

$$\tilde{\boldsymbol{u}}(\boldsymbol{x}) := -\sum_{n=0}^{\infty}\sum_{m=-n}^{n} M_n^m(\widehat{\boldsymbol{x}})\overline{A_n(|\boldsymbol{x}|)}\boldsymbol{\alpha}_n^m, \qquad |\boldsymbol{x}| \geq R. \tag{15}$$

Here $A_n(|\boldsymbol{x}|)$ is defined in (13).

By definition, the operator $\mathcal{T}$ is linear, bounded and one-to-one. As $\boldsymbol{u}$ is an outgoing wave satisfying the Kupradze radiation condition (3), $\tilde{\boldsymbol{u}} = \tilde{\boldsymbol{u}}_p + \tilde{\boldsymbol{u}}_s$ is an incoming wave satisfying the Navier equation (1) and the incoming radiation condition

$$\lim_{r=|\boldsymbol{x}|\to\infty} r\left[\frac{\partial \tilde{\boldsymbol{u}}_\alpha(\boldsymbol{x})}{\partial r} + ik_\alpha \tilde{\boldsymbol{u}}_\alpha(\boldsymbol{x})\right] = 0, \qquad \alpha = p, s.$$

Theorem 3.4. *The OtI mapping* $\mathcal{T}$: Range(G) $\to [\mathrm{L}^2(\mathrm{S_R})]^3$ *takes the explicit form*

$$(\mathcal{T}\boldsymbol{\varphi})(\boldsymbol{x}) = -\frac{1}{R^2}\sum_{n=0}^{\infty}\sum_{m=-n}^{n} M_n^m(\widehat{\boldsymbol{x}})\overline{A_n(R)}\,[A_n(R)]^{-1}\int_{S_R}\overline{M_n^m(\widehat{\boldsymbol{y}})}^{\top}\boldsymbol{\varphi}(\boldsymbol{y})\mathrm{d}s(\boldsymbol{y}). \tag{16}$$

Proof. For each $\boldsymbol{\varphi} \in$ Range(G), we have the expansion

$$\boldsymbol{\varphi}(\boldsymbol{x}) = \sum_{n=0}^{\infty}\sum_{m=-n}^{n} M_n^m(\widehat{\boldsymbol{x}})A_n(R)\boldsymbol{\varphi}_n^m, \qquad |\boldsymbol{x}| = R, \tag{17}$$

where $\boldsymbol{\varphi}_n^m \in \mathbb{C}^3$ and $A_n(R)$ is defined in (13). Clearly,

$$A_n(R)\boldsymbol{\varphi}_n^m = \frac{1}{R^2}\int_{S_R}\overline{M_n^m(\widehat{\boldsymbol{y}})}^{\top}\boldsymbol{\varphi}(\boldsymbol{y})\mathrm{d}s(\boldsymbol{y}).$$

Introduce the matrix $C_n(R) := A_n(R)Q_n(R)$, where the matrix $Q_n(R)$ is defined as

$$Q_n(R) := \begin{pmatrix} R/h_n^{(1)}(k_sR) & 0 & 0 \\ 0 & R/h_n^{(1)}(k_sR) & 0 \\ 0 & 0 & R/h_n^{(1)}(k_pR) \end{pmatrix}.$$

We claim that $h_n^{(1)}(kR) \neq 0$ for all $n > 0, k = k_p, k_s, R > 0$. Otherwise, if there exists some $N \in \mathbb{N}$ such that $h_N^{(1)}(kR) = 0$, then $j_N(kR) = y_N(kR) = 0, k = k_p, k_s, R > 0$. This is contradictory to the Wronskian $W(j_n(t), y_n(t)) = j_n(t)y_n'(t) - j_n'(t)y_n(t) = \frac{1}{t^2}, n \in \mathbb{N}$. Here j_n, y_n denote the spherical Bessel function and spherical Neumann function of order n, respectively. In addition, Lemma 2.15 in [4] shows that the matrix $C_n(R)$ is invertible for all $n \geq 0, R > 0$. Then $A_n(R)$ is invertible which means that

$$\boldsymbol{\varphi}_n^m = \frac{1}{R^2}[A_n(R)]^{-1}\int_{S_R}\overline{M_n^m(\widehat{\boldsymbol{y}})}^{\top}\boldsymbol{\varphi}(\boldsymbol{y})\mathrm{d}s(\boldsymbol{y}). \tag{18}$$

By the definition of $\mathcal{T}$, it follows that

$$(\mathcal{T}\boldsymbol{\varphi})(\boldsymbol{x}) = -\frac{1}{R^2}\sum_{n=0}^{\infty}\sum_{m=-n}^{n} M_n^m(\widehat{\boldsymbol{x}})\overline{A_n(R)}\,[A_n(R)]^{-1}\int_{S_R}\overline{M_n^m(\widehat{\boldsymbol{y}})}^{\top}\boldsymbol{\varphi}(\boldsymbol{y})\mathrm{d}s(\boldsymbol{y}).$$

The proof is complete. □

Next, we consider the expansion of the fundamental solution $\Pi(\boldsymbol{x},\boldsymbol{y})$. Recall (see [6, Theorem 2.11, 6.29]) that $\Phi_k(\boldsymbol{x},\boldsymbol{y})$ and $\Phi_k(\boldsymbol{x},\boldsymbol{y})\mathbf{I}$ have the expansions

$$\Phi_k(\boldsymbol{x},\boldsymbol{y}) = ik\sum_{n=0}^{\infty}\sum_{m=-n}^{n} h_n^{(1)}(k|\boldsymbol{y}|)Y_n^m(\widehat{\boldsymbol{y}})j_n(k|\boldsymbol{x}|)\overline{Y_n^m(\widehat{\boldsymbol{x}})} \tag{19}$$

and

$$\begin{aligned}\Phi_k(\boldsymbol{x},\boldsymbol{y})\mathbf{I} =& ik\sum_{n=1}^{\infty}\sum_{m=-n}^{n} j_n(k|\boldsymbol{x}|)\overline{\boldsymbol{V}_n^m(\widehat{\boldsymbol{x}})}h_n^{(1)}(k|\boldsymbol{y}|)\boldsymbol{V}_n^m(\widehat{\boldsymbol{y}})^\top\\ &+ ik^{-1}\sum_{n=1}^{\infty}\sum_{m=-n}^{n}\nabla\times\left(j_n(k|\boldsymbol{x}|)\overline{\boldsymbol{V}_n^m(\widehat{\boldsymbol{x}})}\right)\nabla\times\left(h_n^{(1)}(k|\boldsymbol{y}|)\boldsymbol{V}_n^m(\widehat{\boldsymbol{y}})\right)^\top\\ &+ ik^{-1}\sum_{n=0}^{\infty}\sum_{m=-n}^{n}\nabla\left(j_n(k|\boldsymbol{x}|)\overline{Y_n^m(\widehat{\boldsymbol{x}})}\right)\nabla\left(h_n^{(1)}(k|\boldsymbol{y}|)Y_n^m(\widehat{\boldsymbol{y}})\right)^\top,\end{aligned} \tag{20}$$

which converge absolutely and uniformly on compact subsets of $|\boldsymbol{x}|<|\boldsymbol{y}|$.

From the relation $\nabla_{\boldsymbol{x}}\nabla_{\boldsymbol{x}}\Phi_k(\boldsymbol{x},\boldsymbol{y}) = -\nabla_{\mathbf{y}}\nabla_{\boldsymbol{x}}\Phi_k(\boldsymbol{x},\boldsymbol{y})$ and $Y_n^m = \overline{Y_n^{-m}}$, we have

$$\begin{aligned}\nabla_{\boldsymbol{x}}\nabla_{\boldsymbol{x}}^\top\Phi_k(\boldsymbol{x},\boldsymbol{y}) &= -ik\sum_{n=0}^{\infty}\sum_{m=-n}^{n}\nabla\left(j_n(k|\boldsymbol{x}|)\overline{Y_n^m(\widehat{\boldsymbol{x}})}\right)\nabla\left(h_n^{(1)}(k|\boldsymbol{y}|)Y_n^m(\widehat{\boldsymbol{y}})\right)^\top\\ &= -ik\sum_{n=0}^{\infty}\sum_{m=-n}^{n}\nabla\left(j_n(k|\boldsymbol{x}|)Y_n^m(\widehat{\boldsymbol{x}})\right)\nabla\left(h_n^{(1)}(k|\boldsymbol{y}|)\overline{Y_n^m(\widehat{\boldsymbol{y}})}\right)^\top.\end{aligned} \tag{21}$$

Combining equations (19) – (21), we obtain the expansion of Π as follows

$$\begin{aligned}\Pi(\boldsymbol{x},\boldsymbol{y}) &= i\sum_{n=0}^{\infty}\sum_{m=-n}^{n}\overline{M_n^m(\widehat{\boldsymbol{x}})}B_n(|\boldsymbol{x}|)\ E\ [A_n(|\boldsymbol{y}|)]^\top M_n^m(\widehat{\boldsymbol{y}})^\top\\ &= i\sum_{n=0}^{\infty}\sum_{m=-n}^{n}M_n^m(\widehat{\boldsymbol{x}})B_n(|\boldsymbol{x}|)\ E\ [A_n(|\boldsymbol{y}|)]^\top\overline{M_n^m(\widehat{\boldsymbol{y}})}^\top,\end{aligned} \tag{22}$$

which converge absolutely and uniformly on compact subsets of $|\boldsymbol{x}|<|\boldsymbol{y}|$. Here, $B_n(|\boldsymbol{x}|)$ and E are defined as

$$B_n(|\boldsymbol{x}|) := \begin{pmatrix} j_n(k_s|\boldsymbol{x}|) & 0 & 0\\ 0 & -\left(j_n(k_s|\boldsymbol{x}|)+k_s|\boldsymbol{x}|j_n'(k_s|\boldsymbol{x}|)\right)/|\boldsymbol{x}| & k_p j_n'(k_p|\boldsymbol{x}|)\\ 0 & -\sqrt{\delta_n}j_n(k_s|\boldsymbol{x}|)/|\boldsymbol{x}| & \sqrt{\delta_n}j_n(k_p|\boldsymbol{x}|)/|\boldsymbol{x}|\end{pmatrix} \tag{23}$$

and

$$E := \begin{pmatrix} k_s/\mu & 0 & 0\\ 0 & 1/(k_s\mu) & 0\\ 0 & 0 & 1/(k_p(\lambda+2\mu))\end{pmatrix}. \tag{24}$$

Lemma 3.5. *$\mathcal{T}\left(\Pi(\cdot,\boldsymbol{z})\boldsymbol{a}|_{S_R}\right) = \overline{\Pi(\cdot,\boldsymbol{z})}\boldsymbol{a}|_{S_R}$ for all $|\boldsymbol{z}|<R$ and $\boldsymbol{a}\in\mathbb{S}^2$.*

Proof. By virtue of $\Pi(\boldsymbol{x},\boldsymbol{z}) = [\Pi(\boldsymbol{x},\boldsymbol{z})]^\top$ and (22), we have for $|\boldsymbol{x}|=R$ that

$$\begin{aligned}\Pi(\boldsymbol{x},\boldsymbol{z}) &= i\sum_{n=0}^{\infty}\sum_{m=-n}^{n}M_n^m(\widehat{\boldsymbol{x}})A_n(R)E^\top\left[B_n(|\boldsymbol{z}|)\right]^\top\overline{M_n^m(\widehat{\boldsymbol{z}})}^\top\\ &= i\sum_{n=0}^{\infty}\sum_{m=-n}^{n}\overline{M_n^m(\widehat{\boldsymbol{x}})}A_n(R)E^\top\left[B_n(|\boldsymbol{z}|)\right]^\top M_n^m(\widehat{\boldsymbol{z}})^\top.\end{aligned} \tag{25}$$

Thus by the definition (16) of $\mathcal{T}$, we have

$$\begin{aligned}&\mathcal{T}\left(\Pi(\cdot,\boldsymbol{z})\boldsymbol{a}|_{S_R}\right)\\&=-\frac{1}{R^2}\sum_{n=0}^{\infty}\sum_{m=-n}^{n}M_n^m(\widehat{\boldsymbol{x}})\overline{A_n(R)}\left[A_n(R)\right]^{-1}\int_{S_R}\overline{M_n^m(\widehat{\boldsymbol{y}})}^{\top}\Pi(\boldsymbol{y},\boldsymbol{z})\boldsymbol{a}\mathrm{d}s(\boldsymbol{y}).\end{aligned}\tag{26}$$

Using the expansion of $\Pi(\boldsymbol{x},\boldsymbol{z})$ in (25), we have

$$\begin{aligned}&\int_{S_R}\overline{M_n^m(\widehat{\boldsymbol{y}})}^{\top}\Pi(\boldsymbol{y},\boldsymbol{z})\boldsymbol{a}\mathrm{d}s(\boldsymbol{y})\\=&i\sum_{l=0}^{\infty}\sum_{q=-l}^{l}\int_{S_R}\overline{M_n^m(\widehat{\boldsymbol{y}})}^{\top}M_l^q(\widehat{\boldsymbol{y}})A_l(R)E^{\top}\left[B_l(|\boldsymbol{z}|)\right]^{\top}\overline{M_l^q(\widehat{\boldsymbol{z}})}^{\top}\boldsymbol{a}\mathrm{d}s(\boldsymbol{y})\\=&i\sum_{l=0}^{\infty}\sum_{q=-l}^{l}\int_{S_R}\overline{M_n^m(\widehat{\boldsymbol{y}})}^{\top}M_l^q(\widehat{\boldsymbol{y}})\mathrm{d}s(\boldsymbol{y})A_l(R)E^{\top}\left[B_l(|\boldsymbol{z}|)\right]^{\top}\overline{M_l^q(\widehat{\boldsymbol{z}})}^{\top}\boldsymbol{a},\end{aligned}\tag{27}$$

where $l,q\in\mathbb{Z}$. Since $\{M_n^m(\theta,\varphi):n=0,1,2\ldots,m=-n.\ldots n\}$ form a complete orthonormal system in $[L^2(\mathbb{S}^2)]^3$, we know that

$$\int_{S_R}\overline{M_n^m(\widehat{\boldsymbol{y}})}^{\top}M_l^q(\widehat{\boldsymbol{y}})\mathrm{d}s(\boldsymbol{y})=\begin{cases}R^2\mathbf{I}, & l=n,\ q=m,\\ \mathbf{0}, & \text{else.}\end{cases}\tag{28}$$

By substituting (28) into (27), we obtain

$$\int_{S_R}\overline{M_n^m(\widehat{\boldsymbol{y}})}^{\top}\Pi(\boldsymbol{y},\boldsymbol{z})\boldsymbol{a}\mathrm{d}s(\boldsymbol{y})=iR^2A_n(R)E^{\top}\left[B_n(|\boldsymbol{z}|)\right]^{\top}\overline{M_n^m(\widehat{\boldsymbol{z}})}^{\top}\boldsymbol{a}.\tag{29}$$

Inserting (29) into (26) gives

$$\mathcal{T}\left(\Pi(\cdot,\boldsymbol{z})\boldsymbol{a}|_{S_R}\right)=-i\sum_{n=0}^{\infty}\sum_{m=-n}^{n}M_n^m(\widehat{\boldsymbol{x}})\overline{A_n(R)}E^{\top}\left[B_n(|\boldsymbol{z}|)\right]^{\top}\overline{M_n^m(\widehat{\boldsymbol{z}})}^{\top}\boldsymbol{a}.\tag{30}$$

As matrices E and B_n are real-valued, it's easy to find that $\mathcal{T}\left(\Pi(\cdot,\boldsymbol{z})\boldsymbol{a}\right)=\overline{\Pi(\cdot,\boldsymbol{z})\boldsymbol{a}}$. □

Lemma 3.6. *The adjoint operator $\mathcal{T}^*:[L^2(S_R)]^3\to[L^2(S_R)]^3$ is given by*

$$\begin{aligned}&(\mathcal{T}^*\boldsymbol{\varphi})(\boldsymbol{x})\\&:=-\frac{1}{R^2}\sum_{n=0}^{\infty}\sum_{m=-n}^{n}M_n^m(\widehat{\boldsymbol{x}})\left[\overline{A_n(R)}^{-1}\right]^{\top}\left[A_n(R)\right]^{\top}\int_{S_R}\overline{M_n^m(\widehat{\boldsymbol{y}})}^{\top}\boldsymbol{\varphi}(\boldsymbol{y})\mathrm{d}s(\boldsymbol{y}).\end{aligned}\tag{31}$$

Moreover, $\mathcal{T}^*$ is injective.

Proof. For each $\boldsymbol{\varphi}(\boldsymbol{x})\in[L^2(S_R)]^3$, we have the expansion

$$\boldsymbol{\varphi}(\boldsymbol{x})=\sum_{n=0}^{\infty}\sum_{m=-n}^{n}M_n^m(\widehat{\boldsymbol{x}})\boldsymbol{\varphi}_n^m\quad\text{with}\quad\boldsymbol{\varphi}_n^m=\frac{1}{R^2}\int_{S_R}\overline{M_n^m(\widehat{\boldsymbol{y}})}^{\top}\boldsymbol{\varphi}(\boldsymbol{y})\mathrm{d}s(\boldsymbol{y})\in\mathbb{C}^3.\tag{32}$$

Observing that

$$||\boldsymbol{\varphi}||^2_{[L^2(S_R)^3]}=R^2\sum_{n=0}^{\infty}\sum_{m=-n}^{n}||\boldsymbol{\varphi}_n^m||^2_{L^2}.$$

If $\mathcal{T}^*\boldsymbol{\varphi}=\mathbf{0}$, then

$$||\mathcal{T}^*\boldsymbol{\varphi}||^2_{[L^2(S_R)^3]}=R^2\sum_{n=0}^{\infty}\sum_{m=-n}^{n}\left|\left|\left[\overline{A_n(R)}^{-1}\right]^{\top}\left[A_n(R)\right]^{\top}\boldsymbol{\varphi}_n^m\right|\right|^2_{L^2}=0,$$

which means that $\left[\overline{A_n(R)}^{-1}\right]^\top [A_n(R)]^\top \boldsymbol{\varphi}_n^m = \mathbf{0}$. It's obvious that $\boldsymbol{\varphi}_n^m = \mathbf{0}$, which implies that $\boldsymbol{\varphi}(\boldsymbol{x}) = \mathbf{0}$. □

3.3. **Factorization of $\mathcal{T}N$.** In this subsection, we multiply the near-field operator N with the OtI operator $\mathcal{T}$ and give a factorization of $\mathcal{T}N$. First, we introduce the single-layer integral operator S and the single-layer potential V by

$$(S\boldsymbol{\psi})(\boldsymbol{x}) = \int_{\partial D} \Pi(\boldsymbol{x},\boldsymbol{y})\boldsymbol{\psi}(\boldsymbol{y})\mathrm{d}s(\boldsymbol{y}), \qquad \boldsymbol{x}\in\partial D,$$
$$(V\boldsymbol{\psi})(\boldsymbol{x}) = \int_{\partial D} \Pi(\boldsymbol{x},\boldsymbol{y})\boldsymbol{\psi}(\boldsymbol{y})\mathrm{d}s(\boldsymbol{y}), \qquad \boldsymbol{x}\in\mathbb{R}^3,$$

where $\boldsymbol{\psi}\in[H^{-\frac{1}{2}}(\partial D)]^3$.

Let the operators H, H^* and G be defined as in Section 3.1. The adjoint operator H^* can be factorized in terms of $\mathcal{T}, G$ and S as follows.

Theorem 3.7. *$H^* = \mathcal{T}GS$.*

Proof. Using the expansion of Π in (22), we obtain an expression of $\boldsymbol{v}_{\boldsymbol{g}}^{in}$ as follows:

$$\boldsymbol{v}_{\boldsymbol{g}}^{in}(\boldsymbol{x}) = i\sum_{n=0}^{\infty}\sum_{m=-n}^{n} M_n^m(\widehat{\boldsymbol{x}})B_n(|\boldsymbol{x}|)\ E\ [A_n(R)]^\top \int_{S_R} \overline{M_n^m(\widehat{\boldsymbol{y}})}^\top \boldsymbol{g}(\boldsymbol{y})\mathrm{d}s(\boldsymbol{y}),\ |\boldsymbol{x}|<R, \tag{33}$$

which together with the definition of H implies

$$(H\boldsymbol{g})(\boldsymbol{x}) = i\sum_{n=0}^{\infty}\sum_{m=-n}^{n} M_n^m(\widehat{\boldsymbol{x}})B_n(|\boldsymbol{x}|)\ E\ [A_n(R)]^\top \int_{S_R} \overline{M_n^m(\widehat{\boldsymbol{y}})}^\top \boldsymbol{g}(\boldsymbol{y})\mathrm{d}s(\boldsymbol{y}),\ \boldsymbol{x}\in\partial D. \tag{34}$$

Since j_n is real valued, the adjoint operator H^* takes the form

$$(H^*\boldsymbol{\psi})(\boldsymbol{x}) = -i\sum_{n=0}^{\infty}\sum_{m=-n}^{n} M_n^m(\widehat{\boldsymbol{x}})\overline{A_n(R)}\int_{\partial D} E^\top [B_n(|\boldsymbol{y}|)]^\top \overline{M_n^m(\widehat{\boldsymbol{y}})}^\top \boldsymbol{\psi}(\boldsymbol{y})\mathrm{d}s(\boldsymbol{y}), \tag{35}$$

for $\boldsymbol{x}\in S_R$, $\boldsymbol{\psi}\in[H^{-\frac{1}{2}}(\partial D)]^3$. Obviously, $V\boldsymbol{\psi}$ is a radiating solution to the Navier equation (1). It follows from the expansion of Π in (22) that for $|\boldsymbol{x}|\geq R$,

$$(V\boldsymbol{\psi})(\boldsymbol{x}) = i\sum_{n=0}^{\infty}\sum_{m=-n}^{n} M_n^m(\widehat{\boldsymbol{x}})A_n(|\boldsymbol{x}|)\int_{\partial D} E^\top [B_n(|\boldsymbol{y}|)]^\top \overline{M_n^m(\widehat{\boldsymbol{y}})}]^\top \boldsymbol{\psi}(\boldsymbol{y})\mathrm{d}s(\boldsymbol{y}).$$

Since $(V\boldsymbol{\psi})(\boldsymbol{x})|_{\partial D} = (S\boldsymbol{\psi})(\boldsymbol{x})$, it's obvious that

$$(GS\boldsymbol{\psi})(\boldsymbol{x}) = i\sum_{n=0}^{\infty}\sum_{m=-n}^{n} M_n^m(\widehat{\boldsymbol{x}})A_n(R)\int_{\partial D} E^\top [B_n(|\boldsymbol{y}|)]^\top \overline{M_n^m(\widehat{\boldsymbol{y}})}]^\top \boldsymbol{\psi}(\boldsymbol{y})\mathrm{d}s(\boldsymbol{y}).$$

Recalling the definition of $\mathcal{T}$, we can verify that $H^* = \mathcal{T}GS$. The proof is complete. □

By Theorem 3.7 and the definition of the operators $\mathcal{T}, G, S$, the operator $\mathcal{T}N$ can be factorized as follows.

Theorem 3.8. *(i) The near-field operator N has the factorization*

$$\mathcal{T}N = -\mathcal{G}S^*\mathcal{G}^*, \qquad \mathcal{G} := \mathcal{T}G. \tag{36}$$

(ii) The operator $\mathcal{G} : [H^{\frac{1}{2}}(\partial D)]^3 \to [L^2(S_R)]^3$ is compact with a dense range in $[L^2(S_R)]^3$.

Proof. (i) By (11), we have $N = -GH$. By Theorem 3.7, $H = S^*G^*\mathcal{T}^* = S^*\mathcal{G}^*$. Hence $\mathcal{T}N = -\mathcal{T}GH = -\mathcal{T}GS^*G^*\mathcal{T}^* = -\mathcal{G}S^*\mathcal{G}^*$. The proof is complete.
(ii) As $\mathcal{T}^*$ is injective, the bounded operator $\mathcal{T}$ has a dense range in $[L^2(S_R)]^3$ by Theorem 4.6 in [6]. Together with Theorem 3.2, one can find that $\mathcal{G} = \mathcal{T}G$ is compact with a dense range in $[L^2(S_R)]^3$. □

Throughout this paper, we define the function $\boldsymbol{\phi}_{\boldsymbol{z}}^{\boldsymbol{a}}(\cdot) = \overline{\Pi(\cdot, \boldsymbol{z})}\boldsymbol{a}|_{S_R} \in [L^2(S_R)]^3$, $\boldsymbol{a} \in \mathbb{S}^2$.

Lemma 3.9. *For $\boldsymbol{z} \in B_R$ and $\boldsymbol{a} \in \mathbb{S}^2$, $\boldsymbol{z} \in D$ if and only if $\boldsymbol{\phi}_{\boldsymbol{z}}^{\boldsymbol{a}}$ belongs to the range of $\mathcal{G}$.*

Proof. For $\boldsymbol{z} \in D$, the function $\boldsymbol{u}(\boldsymbol{x}) := \Pi(\boldsymbol{x}, \boldsymbol{z})\boldsymbol{a}, \boldsymbol{x} \in D^c$, is the unique radiating solution to the scattering problem (1) − (3) with the boundary condition $\boldsymbol{f}(\boldsymbol{x}) := \Pi(\boldsymbol{x}, \boldsymbol{z})\boldsymbol{a}|_{\partial D}$. It follows form the definition of $\mathcal{G}$ and Lemma 3.5 that $(\mathcal{G}\boldsymbol{f})(\boldsymbol{x}) = \overline{\Pi(\boldsymbol{x}, \boldsymbol{z})}\boldsymbol{a}, \boldsymbol{x} \in S_R$. That is $\boldsymbol{\phi}_{\boldsymbol{z}}^{\boldsymbol{a}} \in \text{Range}(\mathcal{G})$.

On the other hand, let $\boldsymbol{z} \in D^c$ and assume that $\mathcal{G}\boldsymbol{f} = \boldsymbol{\phi}_{\boldsymbol{z}}^{\boldsymbol{a}}$ for some $\boldsymbol{f} \in [H^{\frac{1}{2}}(\partial D)]^3$. Let $\boldsymbol{v}$ be the unique radiating solution to the scattering problem (1)−(3) with the boundary condition $\boldsymbol{v} = \boldsymbol{f}$ on ∂D. Since the operator $\mathcal{T}$ is injective, $\mathcal{G}\boldsymbol{f} = \boldsymbol{\phi}_{\boldsymbol{z}}^{\boldsymbol{a}}$ means that $(G\boldsymbol{f})(\boldsymbol{x}) = \Pi(\boldsymbol{x}, \boldsymbol{z})\boldsymbol{a}|_{S_R}$. Thus, we get $\boldsymbol{v}(\boldsymbol{x}) = \Pi(\boldsymbol{x}, \boldsymbol{z})\boldsymbol{a}$ for $|\boldsymbol{x}| \geq R$ due to the uniqueness of the exterior Dirichlet problem. Therefore $\boldsymbol{v}(\boldsymbol{x}) = \Pi(\boldsymbol{x}, \boldsymbol{z})\boldsymbol{a}$ in $D^c \setminus \{\boldsymbol{z}\}$, which contradicts with the analyticity of $\boldsymbol{v}$ in D^c. At last, if $\boldsymbol{z} \in \partial D$, it holds that $\Pi(\cdot, \boldsymbol{z})\boldsymbol{a}|_{\partial D} \notin [H^{\frac{1}{2}}(\partial D)]^3$, which contradicts with the fact that $\boldsymbol{v}|_{\partial D} \in [H^{\frac{1}{2}}(\partial D)]^3$. Hence, $\boldsymbol{z} \in D$. □

Next we present some properties of the single-layer operator S (see [1, Lemmas 6.1, 6.2]), which extend the results [6, Lemma 5.37] from acoustic scattering to the elastic case in $3D$.

Lemma 3.10. *Assume that ω^2 is not the Dirichlet eigenvalue of the operator $-\Delta^*$ in D. Then*
(i) The single-layer operator $S : [H^{-\frac{1}{2}}(\partial D)]^3 \to [H^{\frac{1}{2}}(\partial D)]^3$ is an isomorphism.
(ii) $Im\langle \boldsymbol{\psi}, S\boldsymbol{\psi}\rangle < 0$ for $\boldsymbol{\psi} \in [H^{-\frac{1}{2}}(\partial D)]^3$ with $\boldsymbol{\psi} \neq 0$. Here, $\langle \cdot, \cdot \rangle$ denotes the duality between $[H^{-\frac{1}{2}}(\partial D)]^3$ and $[H^{\frac{1}{2}}(\partial D)]^3$.
(iii) Let $S_i : H^{-\frac{1}{2}}(\partial D)^3 \to H^{\frac{1}{2}}(\partial D)^3$ be the single-layer operator for the frequency $\omega = i$. Then S_i is compact, self-adjoint, and coercive.
(iv) The difference $S - S_i : [H^{-\frac{1}{2}}(\partial D)]^3 \to [H^{\frac{1}{2}}(\partial D)]^3$ is compact.

Relying on properties of the operators $\mathcal{G}$ and S (see Lemmas 3.9 and 3.10), the following range identity [15, Theorem 2.15] can be applied to the operator $\mathcal{T}N$. For an operator F, the operator$F_\sharp$ is defined as $F_\sharp := |\text{Re}[\exp(it)F]| + |\text{Im}F|$ for some $t > 0$.

Lemma 3.11. *Let $X \subset U \subset X^*$ be a Gelfand triple with a Hilbert space U and a reflexive Banach space X such that the imbedding is dense. Furthermore, let Y be a second Hilbert space and let $F : Y \to Y, G : X \to Y$ and $T : X^* \to X$ be linear bounded operators such that $F = GTG^*$. Assume that*
(A1) G is compact with dense range.
(A2) There exists $t \in [0, 2\pi]$ such that $\text{Re}[\exp(it)T]$ has the form $\text{Re}[\exp(it)T] = T_0 + T_1$ with some compact operator T_1 and some self-adjoint and coercive operator $T_0 : X^* \to X$, i.e., there exists $c > 0$

$$\langle \varphi, T_0\varphi\rangle \geq c||\varphi||^2 \qquad \text{for all} \quad \varphi \in X^*.$$

(A3) ImT is compact and non-negative on Range$(G^*) \subset X^*$, i.e., $\langle \varphi, (\mathrm{Im}T)\varphi \rangle \geq 0$ for all $\varphi \in$ Range$(G*)$.
(A4) Re$[\exp(it)T]$ is one-to-one or ImT is strictly positive on the closure $\overline{\text{Range}(G^*)}$ of Range(G^*), i.e.,$\langle \varphi, (\mathrm{Im}T)\varphi \rangle) > 0$ for all $\varphi \in \overline{\text{Range}(G^*)}$ with $\varphi \neq 0$.

Then the operator $F_\sharp$ is positive, and the ranges of $G : X \to Y$ and $F_\sharp^{1/2} : Y \to Y$ coincide.

Applying Lemma 3.11, we have the following result.

Theorem 3.12. *Assume that ω^2 is not the Dirichlet eigenvalue of the operator $-\Delta^*$ in D. Let $\boldsymbol{z} \in B_R$ and $\boldsymbol{\phi}_{\boldsymbol{z}}^{\boldsymbol{a}}$ be given in Lemma 3.9. Denote by $\lambda_j \in \mathbb{C}$ the eigenvalues of the operator*
$(\mathcal{T}N)_\sharp$ with the corresponding normalized eigenfunctions $\boldsymbol{\psi}_j \in [L^2(S_R)]^3$. Then
(i) $\boldsymbol{z} \in D$ if and only if $\boldsymbol{\phi}_{\boldsymbol{z}}^{\boldsymbol{a}}$ belongs to the range Range $\left((\mathcal{T}\mathrm{N})_\sharp^{1/2}\right)$ *of $(\mathcal{T}N)_\sharp^{1/2}$.*
(ii) $\boldsymbol{z} \in D$ if and only if

$$W^{\boldsymbol{a}}(\boldsymbol{z}) := \left[\sum_{j=1}^{\infty} \frac{|\langle \boldsymbol{\phi}_{\boldsymbol{z}}^{\boldsymbol{a}}, \boldsymbol{\psi}_j \rangle_{[L^2(S_R)]^3}|^2}{|\lambda_j|} \right]^{-1} > 0. \tag{37}$$

Proof. Set $t = 0, F = \mathcal{T}N, G = \mathcal{G}, T = S^*, T_0 = S_i, T_1 = \mathrm{Re}(\mathrm{S} - \mathrm{S_i}), \mathrm{X} = \mathrm{H}^{\frac{1}{2}}(\partial \mathrm{D})^3$ and $Y = [L^2(S_R)]^3$. Then application of Lemmas 3.9, 3.10 and 3.11 gives (i). The assertion (ii) follows from Picard's range criterion [6, Theorem 4.8]. □

By Lemma 3.9, one can choose any vector $\boldsymbol{a} \in \mathbb{S}^2$ in Theorem 3.12. For multiple vectors $\{\boldsymbol{a}_i \in \mathbb{S}^2 : j = 1, 2, 3\}$, we define the following indicator function:

$$W(\boldsymbol{z}) = \left[\sum_{j=1}^{3} \frac{1}{W^{\boldsymbol{a}_j}(\boldsymbol{z})} \right]^{-1}, \qquad \boldsymbol{z} \in B_R. \tag{38}$$

Corollary 3.13. *$\boldsymbol{z} \in D$ if and only if $W(\boldsymbol{z}) > 0$.*

Proof. If $\boldsymbol{z} \in D$, Theorem 3.12 implies that $0 < W^{\boldsymbol{a}_j}(\boldsymbol{z}) < \infty$ for all $j = 1, 2, 3$, and thus $W(\boldsymbol{z}) > 0$. On the other hand, if $\boldsymbol{z} \notin D$, again applying Theorem 3.12 gives $W^{\boldsymbol{a}_j}(\boldsymbol{z}) = 0$ for all $j = 1, 2, 3$, implying that $W(\boldsymbol{z}) = 0$. □

4. Numerical experiments in $\mathbb{R}^2$.

In this section, we present some numerical examples in $\mathbb{R}^2$ to illustrate the applicability and effectiveness of our inversion schemes.

4.1. OtI operator in 2D.

We first give the outgoing-to-incoming operator $\mathcal{T}$ in $\mathbb{R}^2$. By employing the polar coordinates we write $\boldsymbol{x} = (r\cos\theta_{\boldsymbol{x}}, r\sin\theta_{\boldsymbol{x}})$. According to the Hodge decomposition, we can introduce scalar functions $\varphi(r, \theta_{\boldsymbol{x}})$ and $\psi(r, \theta_{\boldsymbol{x}})$ such that the scattered field $\boldsymbol{u}$ has the form

$$\boldsymbol{u}(r, \theta_{\boldsymbol{x}}) = \mathrm{grad}\ \varphi(r, \theta_{\boldsymbol{x}}) + \mathrm{curl}\ \psi(r, \theta_{\boldsymbol{x}}), \tag{39}$$

where curl $f = (-\partial_2 f, \partial_1 f)^\top$ and $\varphi(r, \theta_{\boldsymbol{x}})$, $\psi(r, \theta_{\boldsymbol{x}})$ are radiating solutions to the Helmholtz equation.

Recall the relationship between the Cartesian and polar coordinates for gradient:

$$\begin{pmatrix} \partial_1 \\ \partial_2 \end{pmatrix} = \begin{pmatrix} \cos\theta_{\boldsymbol{x}} & -\frac{1}{r}\sin\theta_{\boldsymbol{x}} \\ \sin\theta_{\boldsymbol{x}} & \frac{1}{r}\cos\theta_{\boldsymbol{x}} \end{pmatrix} \begin{pmatrix} \partial_r \\ \partial_\theta \end{pmatrix}.$$

Then radiating solutions $\varphi(r,\theta_{\boldsymbol{x}})$ and $\psi(r,\theta_{\boldsymbol{x}})$ can be expanded into

$$\varphi(r,\theta_{\boldsymbol{x}})=\sum_{n\in\mathbb{Z}}\alpha_n H_n^{(1)}(k_p r)e^{in\theta_{\boldsymbol{x}}},\quad \psi(r,\theta_{\boldsymbol{x}})=\sum_{n\in\mathbb{Z}}\beta_n H_n^{(1)}(k_s r)e^{in\theta_{\boldsymbol{x}}},\tag{40}$$

where $H_n^{(1)}(k_p r), H_n^{(1)}(k_s r)$ are Hankel functions of first kind of order n and $\alpha_n,\beta_n\in\mathbb{C}$ are coefficients.

Combining (39) and (40), we get

$$\boldsymbol{u}(r,\theta_{\boldsymbol{x}})=\sum_{n\in\mathbb{Z}}M(\theta_{\boldsymbol{x}})^\top A_n(r)(\alpha_n,\beta_n)^\top e^{in\theta_{\boldsymbol{x}}},\tag{41}$$

where matrices $M(\theta_{\boldsymbol{x}})$ and $A_n(r)$ are defined as

$$M(\theta_{\boldsymbol{x}})=\begin{pmatrix}\cos\theta_{\boldsymbol{x}} & \sin\theta_{\boldsymbol{x}}\\ -\sin\theta_{\boldsymbol{x}} & \cos\theta_{\boldsymbol{x}}\end{pmatrix},\quad A_n(r)=\begin{pmatrix}k_p H_n^{(1)'}(k_p r) & -inH_n^{(1)}(k_s r)/r\\ inH_n^{(1)}(k_p r)/r & k_s H_n^{(1)'}(k_s r)\end{pmatrix}.$$

The fundamental solution to the Navier equation in $\mathbb{R}^2$ is

$$\Pi(\boldsymbol{x},\boldsymbol{y})=\frac{1}{\mu}\Phi_{k_s}(\boldsymbol{x},\boldsymbol{y})\mathbf{I}+\frac{1}{\omega^2}\nabla_{\boldsymbol{x}}\nabla_{\boldsymbol{x}}^\top[\Phi_{k_s}(\boldsymbol{x},\boldsymbol{y})-\Phi_{k_p}(\boldsymbol{x},\boldsymbol{y})],\qquad \boldsymbol{x}\neq\boldsymbol{y},\tag{42}$$

where $\mathbf{I}$ stands for the unit matrix and $\Phi_k(\boldsymbol{x},\boldsymbol{y})=\dfrac{i}{4}H_0^{(1)}(k|\boldsymbol{x}-\boldsymbol{y}|)$ is the free-space fundamental solution to the Helmholtz equation $(\Delta+k^2)u=0$ in $\mathbb{R}^2$.

Recall the definition of OtI operator $\mathcal{T}$ in $\mathbb{R}^3$, the two-dimensional outgoing-to-incoming operator $\mathcal{T}$ can be represented as

$$(\mathcal{T}\boldsymbol{\varphi})(\boldsymbol{x}):=\int_{S_R}K(\boldsymbol{x},\boldsymbol{y})\boldsymbol{\varphi}(\boldsymbol{y})\mathrm{d}s(\boldsymbol{y}),\quad \boldsymbol{\varphi}(\boldsymbol{x})\in[L^2(S_R)]^2,\tag{43}$$

where the integral kernel $K(\boldsymbol{x},\boldsymbol{y})$ is defined as

$$K(\boldsymbol{x},\boldsymbol{y}):=-\frac{1}{2\pi R}\sum_{n\in\mathbb{Z}}[M(\theta_{\boldsymbol{x}})]^\top B_n(R)A_n(R)^{-1}M(\theta_{\boldsymbol{y}})e^{in(\theta_{\boldsymbol{x}}-\theta_{\boldsymbol{y}})}$$

and

$$B_n(R)=\begin{pmatrix}k_p\overline{H_n^{(1)'}(k_p R)} & -in\overline{H_n^{(1)}(k_s R)}/R\\ in\overline{H_n^{(1)}(k_p R)}/r & k_s\overline{H_n^{(1)'}(k_s R)}\end{pmatrix}.$$

In our numerical implementation, the operator $\mathcal{T}$ is approximated by the truncated operator

$$(\mathcal{T}_{M_1}\boldsymbol{\varphi})(\boldsymbol{x}):=\int_{S_R}K_{M_1}(\boldsymbol{x},\boldsymbol{y})\boldsymbol{\varphi}(\boldsymbol{y})\mathrm{d}s(\boldsymbol{y}),\quad \boldsymbol{\varphi}(\boldsymbol{x})\in[L^2(S_R)]^2,$$

with the kernel given by

$$K_{M_1}(\boldsymbol{x},\boldsymbol{y}):=-\frac{1}{2\pi R}\sum_{n=-M_1}^{n=M_1}[M(\theta_{\boldsymbol{x}})]^\top B_n(R)A_n(R)^{-1}M(\theta_{\boldsymbol{y}})e^{in(\theta_{\boldsymbol{x}}-\theta_{\boldsymbol{y}})},$$

for some $M_1\in\mathbb{Z}^+$.

4.2. **Numerical examples.** In our simulations, we used the boundary integral equation method to compute the near-field data on S_R. Let $\boldsymbol{a}_1 = (1,0)^\top$ and $\boldsymbol{a}_2 = (0,1)^\top$ denote two incident polarization vectors. Define the step size $\triangle\theta_{\boldsymbol{x}} = \triangle\theta_{\boldsymbol{y}} = 2\pi/M_2$ for some $M_2 \in \mathbb{Z}^+$, that is

$$\theta_{\boldsymbol{x}_j} = (j-1)\triangle\theta_{\boldsymbol{x}}, \qquad \theta_{\boldsymbol{y}_j} = (j-1)\triangle\theta_{\boldsymbol{y}}, \qquad j = 1, 2, \ldots, M_2.$$

We choose $2M_2$ incident point sources as

$$\mathcal{K} = \{\Pi(\boldsymbol{x}, \boldsymbol{y}_j)\boldsymbol{a}_1, \Pi(\boldsymbol{x}, \boldsymbol{y}_j)\boldsymbol{a}_2 : j = 1, 2, \ldots, M_2\},$$

where $\boldsymbol{y}_j = R(\cos\theta_{\boldsymbol{y}_j}, \sin\theta_{\boldsymbol{y}_j})$. Denote by $\boldsymbol{u}(\boldsymbol{x}, \boldsymbol{y}_j; \boldsymbol{a}_1)$ and $\boldsymbol{u}(\boldsymbol{x}, \boldsymbol{y}_j; \boldsymbol{a}_2)$ the scattered fields corresponding to the incident field $\Pi(\boldsymbol{x}, \boldsymbol{y}_j)\boldsymbol{a}_1$ and $\Pi(\boldsymbol{x}, \boldsymbol{y}_j)\boldsymbol{a}_2$, respectively. Then we have the near-field matrix

$$\boldsymbol{N}_{M_2\times 2M_2} = [\boldsymbol{b}_{1,1}, \boldsymbol{b}_{1,2}, \boldsymbol{b}_{2,1}, \boldsymbol{b}_{2,2}, \ldots, \boldsymbol{b}_{M_2,1}, \boldsymbol{b}_{M_2,1}],$$

where

$$\boldsymbol{b}_{j,1} := (\boldsymbol{u}(\boldsymbol{x}_1, \boldsymbol{y}_j; \boldsymbol{a}_1), \boldsymbol{u}(\boldsymbol{x}_2, \boldsymbol{y}_j; \boldsymbol{a}_1), \ldots, \boldsymbol{u}(\boldsymbol{x}_{M_2}, \boldsymbol{y}_j; \boldsymbol{a}_1))^\top \in \mathbb{C}^{M_2\times 1},$$
$$\boldsymbol{b}_{j,2} := (\boldsymbol{u}(\boldsymbol{x}_1, \boldsymbol{y}_j; \boldsymbol{a}_2), \boldsymbol{u}(\boldsymbol{x}_2, \boldsymbol{y}_j; \boldsymbol{a}_2), \ldots, \boldsymbol{u}(\boldsymbol{x}_{M_2}, \boldsymbol{y}_j; \boldsymbol{a}_2))^\top \in \mathbb{C}^{M_2\times 1}.$$

The OtI operator $\mathcal{T}$ is approximated by the following matrix

$$\boldsymbol{\mathcal{T}}_{M_2\times M_2} = (K_{M_1}(\boldsymbol{x}_i, \boldsymbol{y}_j))_{M_2\times M_2},$$

where $K_{M_1}(\boldsymbol{x}_i, \boldsymbol{y}_j)$ is defined as

$$K_{M_1}(i,j) := -\frac{1}{2\pi R}\sum_{n=-M_1}^{n=M_1} [M(\theta_{\boldsymbol{x}_i})]^\top B_n(R) A_n(R)^{-1} M(\theta_{\boldsymbol{y}_j}) e^{in(\theta_{\boldsymbol{x}_i} - \theta_{\boldsymbol{y}_j})},$$

for $i, j = 1, 2, \ldots, M_2$. Define $\boldsymbol{\mathcal{T}N}_{\boldsymbol{M_2\times 2M_2}} := \boldsymbol{\mathcal{T}}_{M_2\times M_2}\boldsymbol{N}_{M_2\times 2M_2}$. The characteristic function W defined in (38) can be approximated by the series

$$W^{\boldsymbol{a}}_{M_2}(\boldsymbol{z}) = \left[\sum_{j=1}^{M_1} \frac{|\langle \boldsymbol{\phi}^{\boldsymbol{a}}_{\boldsymbol{z}}, \boldsymbol{\psi}_j\rangle_{[L^2(S_R)]^3}|^2}{|\lambda_j|}\right]^{-1},$$

where $\boldsymbol{\phi}^{\boldsymbol{a}}_{\boldsymbol{z}} = \{\overline{\Pi(\boldsymbol{x}_1, \boldsymbol{z})}\boldsymbol{a}, \overline{\Pi(\boldsymbol{x}_2, \boldsymbol{z})}\boldsymbol{a}, \ldots, \overline{\Pi(\boldsymbol{x}_{M_2}, \boldsymbol{z})}\boldsymbol{a}\}^\top$ with $\boldsymbol{a} = (\cos\alpha, \sin\alpha)^\top$ and $\{\boldsymbol{\psi}_j, \lambda_j\}_{j=1}^{M_2}$ is an eigensystem of the matrix $\boldsymbol{\mathcal{T}N} := |\mathrm{Re}(\boldsymbol{\mathcal{T}}\mathrm{N})| + |\mathrm{Im}(\boldsymbol{\mathcal{T}}\mathrm{N})|$. To test the stability, we add relative noise to the data

$$\boldsymbol{u}^\delta(\boldsymbol{x}_i, \boldsymbol{y}_j; \boldsymbol{a}_s) = \boldsymbol{u}(\boldsymbol{x}_i, \boldsymbol{y}_j; \boldsymbol{a}_s)(1 + \delta\,\mathrm{rand}), \qquad i, j = 1, 2, \ldots M_2,\ s = 1, 2.$$

where rand are uniformly distributed random numbers in $[-1, 1]$.

In the following experiments, we set $\lambda = 2, \mu = 1, \omega = 10, R = 4, M_1 = 40$ and $M_2 = 64$. We choose two polar vectors as $\boldsymbol{a}_1 = (1,0)^\top$ and $\boldsymbol{a}_2 = (0,1)^\top$.

Example 1. Consider a kite-shaped obstacle, which has the parametric equation

$$\boldsymbol{x}(t) = (\cos t + 0.65\cos(2t) - 0.65,\ 1.5\sin t), \qquad t \in [0, 2\pi].$$

Figure 1 presents reconstruction results from the near-field data with the polarization vector$\boldsymbol{a} = (\cos\alpha, \sin\alpha)^\top, \alpha = 2\pi/3$ and noise level $\delta = 0\%$ in Figure 1(b), $\delta = 5\%$ in Figure 1(c), and $\delta = 10\%$ in figure 1(d). In Figure 2, we set noise level $\delta = 5\%$ to see the reconstruction results with different choice of $\boldsymbol{a} = (\cos\alpha, \sin\alpha)^\top$. The polarization angel α is chosen to be zero in Figure 2(a), $\pi/2$ in Figure 2(b) and $2\pi/3$ in Figure 2(c). Figure 2(d) is a superposition of the results for $\alpha = 0, \pi/2$.

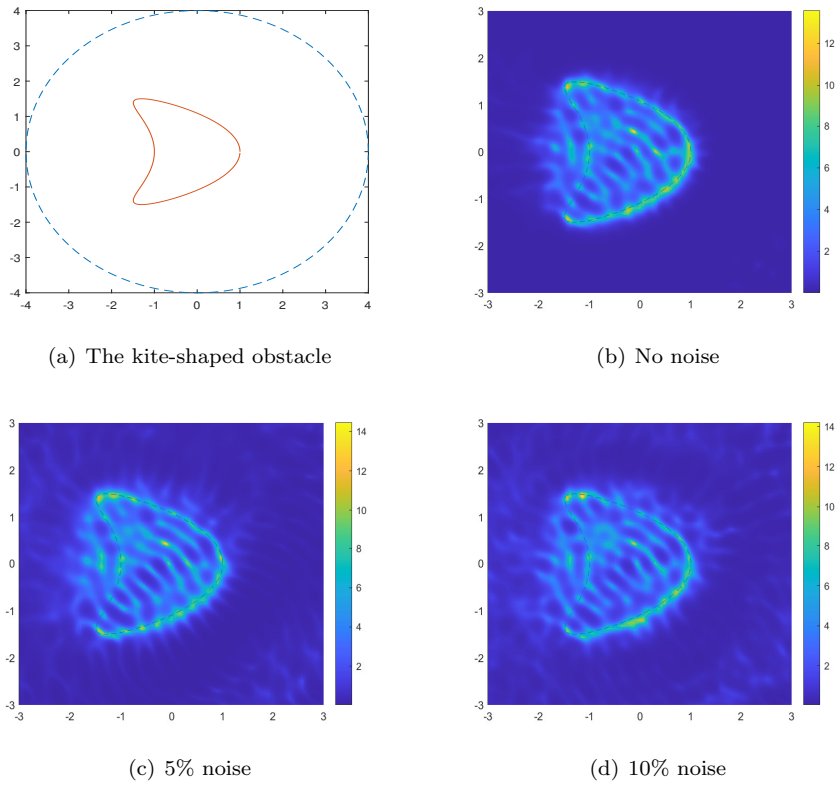

(a) The kite-shaped obstacle

(b) No noise

(c) 5% noise

(d) 10% noise

FIGURE 1. Reconstruction of the kite-shaped obstacle with $\boldsymbol{a} = (\cos\alpha, \sin\alpha)^\top, \alpha = 2\pi/3$.

Example 2. D is given as a star-shaped obstacle with the boundary parameterized by

$$\boldsymbol{x}(t) = (1 + 0.2\cos(5t))\ (\cos t,\ \sin t), \qquad t \in [0, 2\pi].$$

Figure 3 presents the reconstruction results from the true data and noised data at levels 5% and 10%, respectively. Figure 4 shows the results from the data with the noise level at 10% and with different polarization vectors $\boldsymbol{a} = (\cos\alpha, \sin\alpha)^\top$.

Example 3. In the third example, the obstacle D is given by the union of two disjoint components D_1 and D_2. D_1 is a star-shaped obstacle with radius 1 centered at $(2, 2)$, and D_1 is a kite-shaped obstacle with radius 0.5 and centered at $(-1, -1)$. Figure 5 presents the reconstruction results from the data at the noise level 2% and with different polarization vectors $\boldsymbol{a} = (\cos\alpha, \sin\alpha)^\top$.

The numerical examples presented above demonstrate that the indicator function W peaks on the boundaries of the obstacles and can reconstruct the locations and shapes. Unlike the case in acoustics, the behavior of the indicator function is influenced by the polarization vector $\boldsymbol{a}$. For a single obstacle, a single vector $\boldsymbol{a}$ suffices to reconstruct the shape and location. However, in the case of two disconnected components, the reconstructions from one polarization vector don't show complete boundary information. The third example highlights that utilizing near-field data

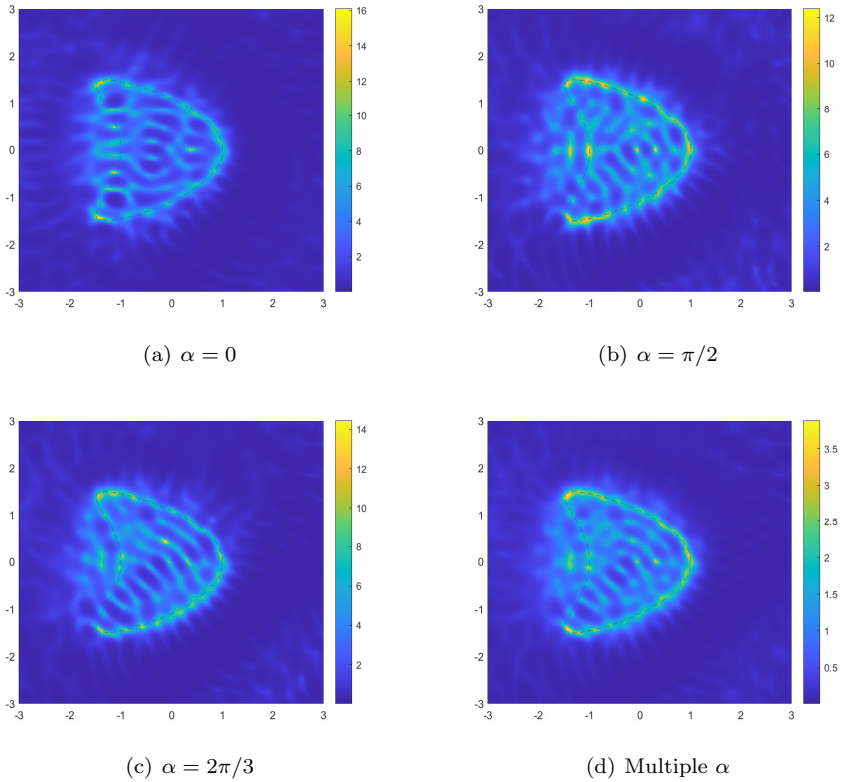

(a) $\alpha = 0$ (b) $\alpha = \pi/2$

(c) $\alpha = 2\pi/3$ (d) Multiple α

FIGURE 2. Reconstruction of the kite-shaped obstacle with different α.

with multiple vectors $\boldsymbol{a}$ enhances the reconstruction quality on the identification of obstacle boundaries.

Acknowledgments. T. Yin acknowledges with thanks support from the National Key R&D Program of China, Grant No. 2024YFA1016000, the Strategic Priority Research Program of the Chinese Academy of Sciences, Grant No. XDB0640000 and NSFC through Grants 12171465 and 12288201. G. Hu is supported by the Beijing Natural Science Foundation (No. Z210001), National Science Foundation (NSFC 12425112) and the Fundamental Research Funds for Central Universities in China (No. 050-63213025). B. Zhang acknowledges with thanks support from NNSFC grant (No. 12431016).

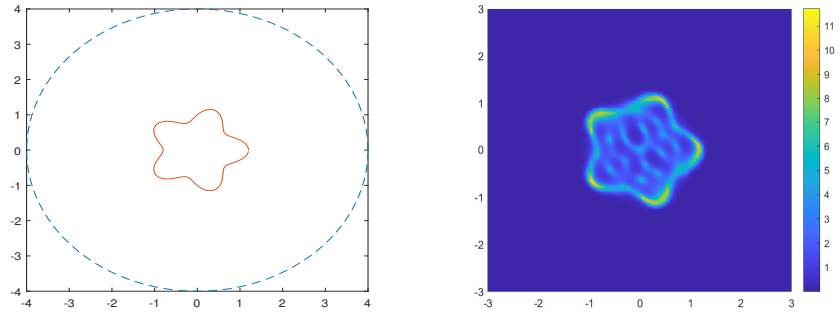

(a) The star-shaped obstacle

(b) No noise

(c) 5% noise

(d) 10% noise

FIGURE 3. Reconstruction of the star-shaped obstacle with $\boldsymbol{a} = (\cos\alpha, \sin\alpha)^\top, \alpha = 2\pi/3$.

REFERENCES

[1] C. J. S. Alves and R. Kress, On the far-field operator in elastic obstacle scattering, *IMA J. Appl. Math.*, **67** (2002), 1–21.

[2] H. Ammari, P. Calmon and E. Iakovleva, Direct elastic imaging of a ismall inclusion, *SIAM J. Imaging Sci.*, **1** (2008), 169–187.

[3] T. Arens, Linear sampling methods for 2D inverse elastic wave scattering, *Inverse Problems*, **17** (2001), 1445-1464.

[4] G. Bao, G. Hu, J. Sun and T. Yin, Direct and inverse elastic scattering from anisotropic media, *J. Math. Pures Appl.*, **117** (2018), 263-301.

[5] Z. Cheng and H. Dong, Uniqueness and reconstruction method for inverse elastic wave scattering with phaseless data, *Inverse Probl. Imaging*, **18** (2024), 406-433.

[6] D. Colton and R. Kress, *Inverse Acoustic and Electromagnetic Scattering Theory*, 3^{nd} edition, Springer, New York, 2013.

[7] J. Elschner and G. Hu, Uniqueness and factorization method for inverse elastic scattering with a single incoming wave, *Inverse Problems*, **35** (2019), 094002, 18 pp.

[8] J. T. Fokkema and P. M. Berg, Elastodynamic diffraction by a periodic rough surface (stress-free boundary), *J. Acoust. Soc. Am.*, **62** (1977), 1095–1101.

[9] P. Hähner and G. C. Hsiao, Uniqueness theorems in inverse obstacle scattering of elastic waves, *Inverse Problems*, **9** (1993), 525-534.

[10] G. Hu, A. Kirsch and M. Sini, Some inverse problems arising from elastic scattering by rigid obstacles, *Inverse Problems*, **29** (2012), 015009, 21 pp.

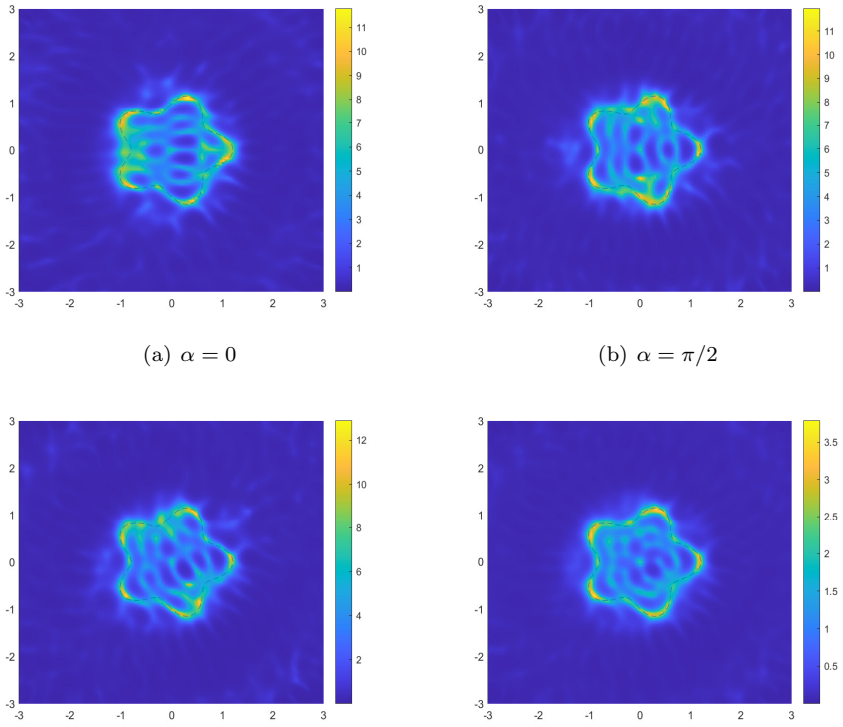

(a) $\alpha = 0$ (b) $\alpha = \pi/2$

(c) $\alpha = 2\pi/3$ (d) Multiple α

FIGURE 4. Reconstruction of the star-shaped obstacle with different α.

[11] G. Hu, J. Yang, B. Zhang and H. Zhang, Near-field imaging of scattering obstacles with the factorization method, *Inverse Problems*, **30** (2014), 095005, 25 pp.
[12] K. Ito, B. Jin and J. Zou, A direct sampling method to an inverse medium scattering problem, *Inverse Problems*, **28** (2012), 025003, 11 pp.
[13] X. Ji, X. Liu and Y. Xi, Direct sampling methods for inverse elastic scattering problems, *Inverse Problems*, **34** (2018), 035008, 22 pp.
[14] A. Kirsch, Characterization of the shape of a scattering obstacle using the spectral data of the far field operator, *Inverse Problems*, **14** (1998), 1489–1512.
[15] A. Kirsch and N. Grinberg, *The Factorization Method for Inverse Problems*, Oxford University Press, Oxford, 2008.
[16] V. D. Kupradze, *Three-Dimensional Problems of the Mathematical Theory of Elasticity and Thermoelasticity*, North-Holland, Amsterdam, 1979.
[17] P. Li, Y. Wang, Z. Wang and Y. Zhao, Inverse obstacle scattering for elastic waves, *Inverse Problems*, **32** (2016), 115018, 24 pp.
[18] P. Li and X. Yuan, Inverse obstacle scattering for elastic waves in three dimensions, *Inverse Probl. Imaging*, **13** (2019), 545–573.
[19] S. Li, J. Lv and Y. Wang, Factorization method for inverse elastic obstacle scattering with neumann boundary condition, *J. Sci. Comput.*, **104** (2025), Paper No. 45, 37 pp.
[20] X. Liu, S. Meng and B. Zhang, Modified sampling method with near field measurements, *SIAM J. Appl. Math.*, **82** (202), 244–266.
[21] J. H. Rose, Elastic wave inverse scattering in nondestructive evaluation, *PAGEOPH*, **131** (1989), 715–739.

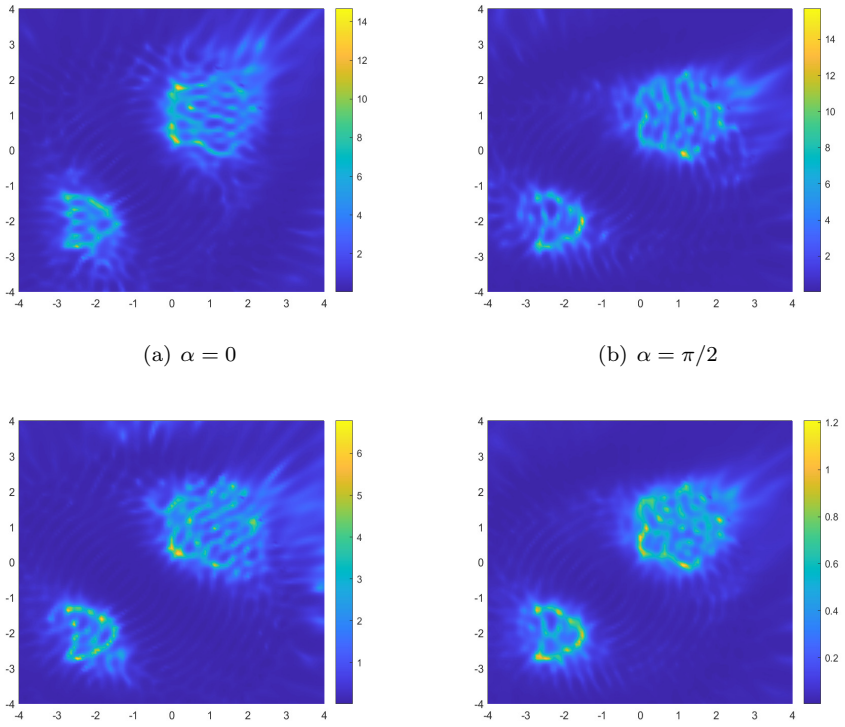

(a) $\alpha = 0$ (b) $\alpha = \pi/2$

(c) $\alpha = 2\pi/3$ (d) Multiple α

FIGURE 5. Reconstruction of two rigid obstacles with different α.

[22] J. W. C. Sherwood, Elastic wave propagation in a semi-infinite solid medium, *Proc. Phys. Soc.*, **7**1 (1958), 207–219.

[23] J. Xiang and G. Yan, The uniqueness of the inverse elastic wave scattering problem based on the mixed reciprocity relation, *Inverse Probl. Imaging*, **15** (2021), 539–554.

[24] J. Xiang and G. Yan, The factorization method for a mixed inverse elastic scattering problem, *IMA J. Appl. Math.*, **87** (2022), 407–437.

[25] T. Yin, G. Hu, L. Xu and B. Zhang, Near-field imaging of obstacles with the factorization method: Fluid–solid interaction, *Inverse Problems*, **32** (2016), 015003, 29 pp.

[26] J. Yue, M. Li, P. Li and X. Yuan, Numerical solution of an inverse obstacle scattering problem for elastic waves via the Helmholtz decomposition, *Commun. Comput. Phys.*, **26** (2019), 809-837.

Received June 2025; revised October 2025; early access October 2025.